PASJ: Publ. Astron. Soc. Japan , –?? (2014)

Theoretical Models of Multi-waveband QSO Luminosity Functions

Takashi Hosokawa[1], Shin Mineshige[2], Toshihiro Kawaguchi[1], Kohji Yoshikawa[1], and Masayuki Umemura[3]
[1]*Department of Astronomy, Graduate School of Science, Kyoto University, Kitashirakawa, Sakyo-ku, Kyoto 606-8502*
E-mail(TH): hosokawa@kusastro.kyoto-u.ac.jp
[2]*Yukawa Institute for Theoretical Physics, Kyoto University, Kitashirakawa, Sakyo-ku, Kyoto 606-8502*
[3]*Center for Computational Physics, University of Tsukuba, 1-1-1 Tennoudai, Tsukuba, Ibaraki 305-8577*

(Received 2001 February; accepted)

arXiv:astro-ph/0107255v2 17 Jul 2001

Abstract

Cosmological evolution of the QSO luminosity functions (LFs) xat NIR/optical/X-ray bands for $1.3 \lesssim z \lesssim 3.5$ is investigated based on the realistic QSO spectra. The accretion-disk theory predicts that although QSO luminosities only depend on mass-accretion rate, $\dot{M}$, QSO spectra have a dependence on black-hole mass, $M_{\rm BH}$, as well. The smaller $M_{\rm BH}$ is and/or the larger $\dot{M}$ is, the harder becomes the QSO NIR/optical/UV spectrum. We model disk spectra which can reproduce these features and calculated LFs for redshift $z \sim 3$ with the assumption of new-born QSOs being shining at the Eddington luminosity. The main results are: (i) the observed LFs at optical and X-rays can be simultaneously reproduced. (ii) LFs at optical and X-ray bands are not sensitive to $M_{\rm BH}$, while LFs at NIR bands are; about one order of magnitude difference is expected in volume number densities at $L_{I,J} \sim 10^{46}{\rm erg\,s^{-1}}$ between the case that all QSOs would have the same spectral shape as that of $M_{\rm BH} = 10^9 M_\odot$ and the case with $M_{\rm BH} = 10^{11} M_\odot$. (iii) The resultant LFs at NIR are dominated by $10^7 M_\odot$ black-holes at $L_{I,J} \lesssim 10^{44}{\rm erg\,s^{-1}}$, and by $10^{11} M_\odot$ black-holes at $L_{I,J} \gtrsim 10^{46}{\rm erg\,s^{-1}}$. Future infrared observations from space(e.g.NGST) will probe cosmological evolution of black hole masses. For redshift $z < 3$, on the other hand, the observed optical/X-ray LFs can be fitted, if the initial QSO luminosity L_0 is below the Eddington luminosity $L_{\rm Edd}$. Interestingly, the best fitting values of $\ell \equiv L_0/L_{\rm Edd}$ are different in B- and X-ray bands; $\ell_{\rm B} \approx 2.5\,\ell_{\rm x}$. The reason for this discrepancy is briefly discussed.

Key words: accretion, accretion disks — black holes — cosmology: theory — galaxies: active — galaxies: Seyfert

1. Introduction

The cosmological evolution of QSOs and QSO black holes attracts many researchers recently thanks to the rapid progress in observational studies of distant QSOs, which promotes intensive discussion on their formation mechanism and formation epochs (e.g., Rees 1984; Haiman & Loeb 1999: hearafter HL99; Kauffmann & Haehnelt 2000; Nulson & Fabian 2000). The efforts have been concentrated on understanding the specific evolutionary behavior of the bright QSO population. It shows a rapid increase from the present day back to redshift $z \sim 2.5$ (Schmidt, Green 1983). It is still controversial whether the comoving density of QSOs remained high at $z > 2.5$, as is suggested by *ROSAT* X-ray studies (Miyaji et al. 1998, 2000) or rapidly decreases toward higher z, as is obtained by optical and radio survey(Pei 1995, see also Osmer 1982; Shaver et al. 1996,1999). This apparent discrepancy may simply imply that X-ray surveys could detect optically faint QSOs whose population shows no rapid decline beyond $z \sim 2.5$ (HL99). It is interesting to note similar evolutionary behavior of the cosmic star-formation history (Madau et al. 1996; Connolly et al. 1997; Glazebrook et al. 1999; Steidel et al. 1999), indicating a close link between the QSO evolution and the cosmic star formation history (Franceschini et al. 1999).

LFs of bright QSOs are well approximated by double power laws (e.g. Boyle et al. 1988). This shape contrasts those of normal galaxies which show exponential decline at high luminosities. Pioneered by Cavaliere & Szalay (1986) and Efstathiou & Rees (1988), theoretical modeling of the QSO LFs has been attempted by several authors; e.g., Haehnelt et al. (1998, hereafter HNR98), Haiman & Loeb (1998, hereafter HL98; HL99), Cavaliere & Vittorini (1998, 2000), and Kauffman & Haehnelt (2000). We specifically pick up models by HNR98 and HL98, who consider formation of black holes in hierarchically growing dark halos, whose formation rate is assumed to be described by the Press-Schechter theory. It is also assumed that each dark halo finally produces one supermassive black hole with mass being a function of mass of its host dark halo, and that QSO black holes

shine at Eddington luminosity for certain period by accreting environmental gas and then quickly fade out as accretion material is depleted. The basic shapes of the LFs in either B-bands or X-rays are then nicely reproduced.

However, these studies assume rather ad hoc accretion spectra which require improvement by using realistic accretion flow models. This is the motivation of the present study. We, here, especially focus our discussion on how to extract information regarding the cosmological evolution of black-hole mass from multi-wavelength LFs.

The basic accretion theory tells that black-hole accretion produces energy output of the order of $0.1\dot{M}c^2$ (with c being speed of light); that is, the disk luminosity, L, does not contain information regarding black-hole mass except for the lower limit of $M_{\rm BH}$ set by the constraint that L should not largely exceed the Eddington luminosity, $L_{\rm Edd} = 1.5 \times 10^{38}(M_{\rm BH}/M_\odot)$erg s^{-1}. We wish to emphasize, however, that spectral energy distribution certainly depends on black-hole mass. This is observationally clear, since galactic black-hole candidates with $M_{\rm BH} \sim 10M_\odot$ exhibit distinct spectra in optical to soft X-ray ranges from those of typical AGNs. Further, there is growing evidence that narrow-line Seyfert 1 galaxies (NLS1s), which are believed to harbor relatively less massive black holes with $M_{\rm BH} \simeq 10^5 - 10^7 M_\odot$, show unique soft X-ray features; i.e., enhanced soft X-ray excess and large spectral index in X-rays (Pounds et al. 1996; Otani et al. 1996; Boller et al. 1996; Brandt et al. 1997).

These features can be basically accounted for in terms of the standard-disk theory (Shakura & Sunyaev 1973) and that with some extension (Mineshige et al. 2000). It is well known that the effective (or surface) temperature of optically thick (standard) disks depends on $M_{\rm BH}$ as

$$T_{\rm eff}(r) \propto \frac{M_{\rm BH}^{1/4}\dot{M}^{1/4}}{r^{3/4}} \propto M_{\rm BH}^{-1/4}\frac{(L/L_{\rm Edd})^{1/4}}{(r/R_{\rm g})^{3/4}}, \qquad (1)$$

that is, the peak frequency of the disk spectral peak shifts in proportion to $M_{\rm BH}^{-1/4} \times (L/L_{\rm Edd})^{1/4}$. The smaller $M_{\rm BH}$ is and/or the larger $\dot{M}$ (or L) is, the harder becomes the QSO optical/UV spectrum. X-ray spectra, in contrast, practically have no mass dependence, since the electron temperature of optically thin, hot plasmas near black holes is in any cases kept around 5×10^9 K regardless of black hole mass. This is explicitly demonstrated in the framework of a model of optically thin, advection-dominated accretion flow (ADAF; Ichimaru 1977, see Manmoto et al. 1997 for the spectrum without self-similar assumptions).

Then, we may be able to extract information concerning black-hole masses as a function of redshift, z, through the comparisons of QSO LFs at two (or more) different wavebands; e.g. X-rays, optical, and infrared bands. This will be a final goal of the present study. The plan of the present paper is as follows: in section 2 we explain our models, which are basically the same as those of HL98 and HNR98 except for adopting realistic QSO spectral models. We then give our resultant LFs at B-, X-ray, and NIR bands for $z \sim 3$ and $z \lesssim 2$ in sections 3 and 4, respectively. The final section is devoted to discussion.

2. Our Models

2.1. Basic assumptions

It is generally believed that most of the mass in the universe is in the form of "dark matter (DM)." Accordingly, the spatial distribution of luminous objects, such as galaxies, QSOs, and so on, is likely to follow that of DM. Therefore, it is reasonable to use the volume number density of dark halos to investigate that of luminous objects, including QSOs. We here adopt two simple models for calculating LFs, following HNR98 and HL98. The basic assumptions made in both models are as follows:

2.1.1. Relation between halo mass and black-hole mass

We assume that each dark halo necessarily has only one supermassive black hole at the center, though it is still controversial observationally. Then, we have

$$M_{\rm BH} = F(M_{\rm halo}) \qquad (2)$$

where $M_{\rm halo}$ is the host dark-halo mass and the function form $F(M)$ depends on models, as prescribed below:

In model A (HNR98), the relation between $M_{\rm BH}$ and $M_{\rm halo}$ is nonlinear;

$$M_{\rm BH} = Cv_{\rm halo}^5 = C' M_{\rm halo}^{5/3}(1+z)^{5/2}, \qquad (3)$$

where C' and C are constants and C is treated as a free parameter. The physical meaning of this relation is described in Silk & Rees (1998). Equation (3) gives a critical black hole mass to bound gas in its host halo against the outward wind from QSO. If black hole mass exceeds this upper limit, QSO could expel all the gas from its host galaxy, and the black hole will never grow further.

In Model B (HL98), in contrast, a linear relation between $M_{\rm BH}$ and $M_{\rm halo}$ is assumed;

$$M_{\rm BH} = \epsilon M_{\rm halo}. \qquad (4)$$

Here, ϵ is a free parameter. This expression is based on the observed linear relation among the bulge luminosity and the black-hole mass (Magorrian et al. 1998, hereafter MG98; see also Laor 1998; Ferrarese & Merritt 2000; Gebhardt et al. 2000).

2.1.2. QSO light curves

We, next, assume that time evolution of the QSO luminosity at high z ($\gtrsim 3$) follows

$$L(t) = L_{\rm Edd}\exp\left(-\frac{t}{t_{\rm Q}}\right) \equiv M_{\rm BH}\ g(t), \qquad (5)$$

where we set $t = 0$ when a halo collapses. Such a simple prescription for a single QSO light curve is known to reproduce well the observed LFs at $z \gtrsim 3$ (HL98, HNR98).

If one directly uses the models described above to calculate QSO LF at $z < 2$, we over-predict number density of QSOs compared to the observed co-moving density of QSOs that exhibits rapid decline towards $z = 0$ from $z \sim 2.5$. Therefore, model assumptions should be reexamined. The rapid decay in the QSO density seems to be caused by the depletion of fueling mass; i.e., environmental gas surrounding a black hole is not enough to shine the black hole at $L_{\rm Edd}$. Hence, it is reasonable to assume that the QSO luminosity should be less than $L_{\rm Edd}$ even at the epoch when its host halo collapses (Mcleod et al. 1999; Haiman & Menou 2000). We thus introduce a parameter, $\ell \equiv L_0/L_{\rm Edd} \leq 1$, and, assuming a relation, $L_0 \propto L_{\rm Edd} \propto M_{\rm BH}$, we set

$$L(t) = L_0 \exp\left(-\frac{t}{t_{\rm Q}}\right) \equiv \ell M_{\rm BH}\ g(t). \tag{6}$$

Considering the evolution of gas content in galaxies due to star formation activity, ℓ will be decreasing towards $z \sim 0$.

2.1.3. Formation rate of dark halo

In previous studies, the formation rate of dark halos and black holes was often regarded as the time derivative of Press-Schechter (PS) mass function (Press & Schechter 1974);

$$\frac{d^2 N_{\rm BH}}{dM_{\rm BH} dz} = \frac{1}{\epsilon}\frac{d}{dz}\frac{dN_{\rm PS}}{dM_{\rm halo}}. \tag{7}$$

At later times (especially at $z \lesssim 2$), however, this is inadequate, since equation (7) gives a negative formation rate for small halo masses. This is because that the time derivative of PS mass function contain two distinct terms: i) the formation rate (which is positive) of halos with mass M from objects with lower masses and ii) the destruction rate (which is negative) due to merging of halos with mass M into objects with higher masses, and the latter dominates over the former at later times for small halo masses. Many authors have attempted to derive the genuine formation rate in various ways (e.g., Lacey & Cole 1993, Sasaki 1994). We here adopt a model proposed by Kitayama & Suto (1996). Then, we regard the formation rate of black holes to be

$$\frac{d^2 N_{\rm BH}}{dM_{\rm BH} dz} = \frac{1}{\epsilon}\frac{d}{dz}\frac{dN_{\rm form}}{dM_{\rm halo}} \times p(z', z). \tag{8}$$

where, $d(dN_{\rm form}/dM_{\rm halo})/dz$ is the formation rate of dark halos, and $p(z', z)$ is the *survival probability*, probability that the dark halo formed at z' remains at z without merging into objects of higher masses. Kitayama & Suto (1996) calculated the genuine formation rate by the merging rate of halos of $< M/2$ into a halo of mass M.

After all, the number of free parameters is three for each model: QSO lifetime, $t_{\rm Q}$, the initial Eddington ratio, ℓ, and the constant related to $M_{\rm BH}$, C (model A) or ϵ (model B). These are to be determined such that the model should reproduce the observational data most successfully.

2.2. QSO Luminosity Functions

Here, we let $\Phi(L, z)dL$ be the number of QSOs per unit comoving volume at redshift z, whose absolute bolometric luminosity is between L and $L + dL$. On the basis of these assumptions described in subsection 2.1.1–2.1.3, QSO LFs, $\Phi(L, z)dL$, can be calculated by the summation of luminosities of all the QSOs whose luminosity is L at redshift z; that is

$$\Phi(L, z) = \int_0^\infty \int^z dM_{\rm BH} dz' \frac{d^2 N_{\rm BH}}{dM_{\rm BH} dz'} \times \delta\left[M_{\rm BH} - \frac{L}{\ell g(t_{z,z'})}\right], \tag{9}$$

where δ is delta-function, $g(t)$ is defined in equation (5), and $t_{z,z'}$ is the time between the epochs of redshifts z and z'. Here, the lower limit of $M_{\rm halo}$ is $M_{\rm halo} \geq 10^8 M_\odot [\,(1+z)/10\,]^{-1.5}$. This corresponds to the virial temperature, $T_{\rm vir} \geq 10^4$K. This is the condition for the gas to sink to the black hole by cooling effect.

Practically, it is convenient to define $L_{\rm band}$, the observational band luminosity. We should note that $L_{\rm band}$ is a function of $M_{\rm BH}$ and $\dot{M}$ in accordance with mass and mass-flow rate dependences of the QSO spectra. We, hereafter, use $\Phi(L_{\rm band}, z)$ rather than $\Phi(L, z)$ and simply write $\Phi(L_{\rm band}, z)$ as $\Phi(L, z)$ below.

The LFs certainly depend on the adopted cosmological model. Though it still remains an open question whether the universe is open or closed, recent observations seem to indicate a flat universe (e.g., de Bernardis et al. 2000). Thus, here we adopt a ΛCDM cosmology with tilted power spectrum, $(\Omega_0, \Omega_\Lambda, \Omega_{\rm b}, h, \sigma_{8h^{-1}}, n) = (0.35, 0.65, 0.04, 0.65, 0.87, 0.96)$, as is suggested by of Ostriker & Steinhardt (1995).

2.3. Adopted QSO Spectra

As discussed before, we need to give disk spectra to calculate band luminosities, $L_{\rm band}$, and thus QSO LFs. Here, we adopt a simple but reasonably realistic model of QSO spectra as displayed in figure 1. These spectra are the sum of three components: emission from a disk-corona structure (at $\lambda < 1\mu$m or $\log\nu > 14.5$), that from an outer optically thick disk (around $\lambda \sim 1\mu$m), and the IR bump (at $\lambda > 1\mu$m). In addition, we simply assume strong photo-electric absorption due to IGM (Especially, Lyman limit systems mainly contributes to absorption here. (Stengler-Larrea et al. 1995)) in the range, 60 Å$\leq \lambda \leq$ 912 Å.

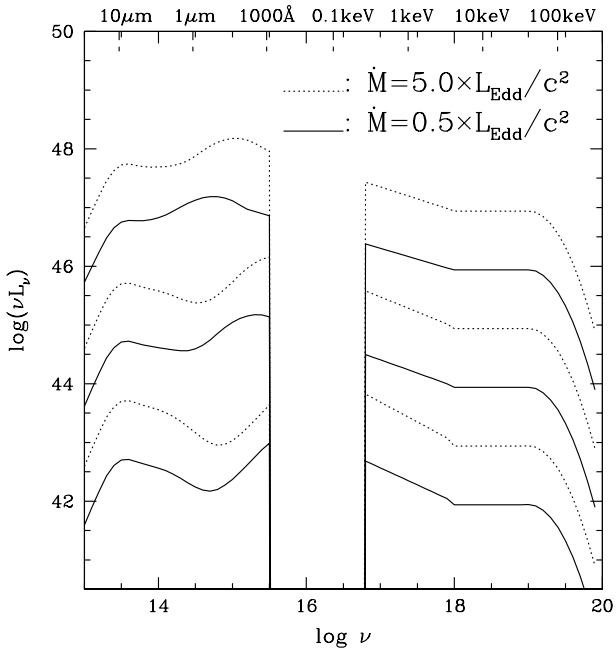

Fig. 1.. The adopted QSO spectra. The solid lines are the cases for $\dot{M} = 0.5 \times L_{\rm Edd}/c^2$, while the dotted lines are for $\dot{M} = 5.0 \times L_{\rm Edd}/c^2$. Three lines of each set represent the spectra for $M_{\rm BH} = 10^{11}, 10^9, 10^7 M_\odot$ from the top downwards.

2.3.1. *Disk-corona component*

The disk-corona model spectrum is the main component at $\lambda \leq 1\mu$m. Here, we use a model by Kawaguchi et al. (2000), since they could, for the first time, reproduce the observed broad-band (optical to hard X-ray) spectral energy distributions of QSOs. The idea is to couple a standard-type disk body with $T_{\rm eff} \sim 10^5 (r/r_{\rm g})^{-3/4}$ K and an advection-dominated disk corona, in which $T_{\rm elec} \sim 10^9$ K. Following Haardt & Maraschi (1991), they assume that a fraction, $1-f$, of energy is dissipated in the disk body, while the remaining fraction, f, is in the coronae. By solving the hydrostatic balance and 1D radiative transfer including inverse-Compton processes for each radius, they finally obtain the spectrum at $4-300 r_{\rm g}$. According to this model, the big blue bump (BBB) is by thermal black body emission from the disk body at small radii,the soft X-ray excess is inverse-Compton scattering of the BBB soft photons in the corona at small radii, and the hard X-rays are bremsstrahlung radiation from the coronae at large radii.

Free parameters involved with this model are $M_{\rm BH}$, $\dot{M}$, f, $\alpha_{\rm c}$, $\tau_{\rm c}$, τ_0, $R_{\rm in}$, $R_{\rm out}$; black-hole mass, accretion rate, fraction of energy dissipated in the corona, viscosity parameter in the corona, coronal optical depth, disk optical depth, inner and outer edges of the corona, respectively. The calibration of this model spectra is made so as to reproduce the so-called QSO composite spectrum (Zheng et al. 1997; Laor et al. 1997), in which the spectral indices ($L_\nu \propto \nu^{-\alpha}$) are $\alpha \sim 0.3$ at optical (1 μm $\geq \lambda \geq$ 2500 Å), $\alpha \sim 1.0$ at UV(2500 Å$\geq \lambda \geq$ 1000 Å), $\alpha \sim 1.8$ at FUV(1000 Å$\geq \lambda$), $\alpha \sim 1.6$ at soft X-ray(0.2–2.0 keV), and $\alpha \sim 0.7$ at hard X-ray($>$ 2.0 keV), and cut-off energy for hard X-ray is about 100 keV. Kawaguchi et al. find that one can reasonably reproduce the observational QSO composite spectrum with parameters of (f, $\alpha_{\rm c}$, τ_c, τ_0, $R_{\rm in}$, $R_{\rm out}$) = (0.6, 1.0, 0.6, 1000, $4.0 R_{\rm g}$, $300 R_{\rm g}$), $M_{\rm BH} = 3\times10^9 M_\odot$ and $\dot{M} = 0.5\times L_{\rm Edd}/c^2$. Note that $\dot{M}$ of $12 L_{\rm Edd}/c^2$ corresponds to a disk with $L_{\rm Edd}$. The frequency at which the BBB reaches its peak flux varies as $M_{\rm BH}^{-1/4}$ as in the standard disk model, since the main component of BBB is the thermal emission from the optically thick disk [see equation (1)].

Mass accretion rate is assumed to change according to equation (5). Thus, the spectral shape also changes with the time elapsed after a halo collapses. The spectra for different $M_{\rm BH}$ and $\dot{M}$ are calculated according to the disk corona model with the same parameter set given above. As $\dot{M}$ decreases and/or $M_{\rm BH}$ increases, the spectral peak shifts towards longer wavelength regimes, as $\dot{M}/L_{\rm Edd}{}^{-1/4}$ and $M_{\rm BH}^{1/4}$ (Figure 1). These dependences are the same as that of the standard disk. Since optical/NIR spectral index α is ~ 0.3, luminosity those bands varies as $M_{\rm BH}^{1.2}$ with fixed $\dot{M}/L_{\rm Edd}$. The X-ray luminosity is in proportion to $M_{\rm BH}$, on the other hand.

2.3.2. *Outer optically thick part*

In addition, we consider the spectrum of the standard disk at larger radii ($r > 300\ R_{\rm g}$), assuming that disk corona only exists inside 300 $R_{\rm g}$. This component appears between the IR bump and the BBB in the spectrum. For the total disk size of $1000 R_{\rm g}$, the spectral index of the standard disk is $\alpha \sim -0.3$ at this wavelength.

2.3.3. *IR bump*

The second component is the IR bump, typically extending from (20–30) to 1 μm (Telesco et al. 1984; Radovich et al. 1999). At the present, it is widely believed that the dust thermal emission is responsible for this bump. A supporting evidence is that the higher energy end of the bump is found at ~ 1 μm, corresponding to a temperature of ~ 1800 K, at which dust sublimates (e.g., Kobayashi et al. 1993). Here, we assume that the spectral indices of $\alpha = 1.4$ at $\lambda < 10$ μm (Neugebauer et al. 1987; Polletta & Courvoisier 1999), and $\alpha = -2.0$ at $\lambda > 10$ μm (Rayleigh-Jeans regime), and that the total IR power varies with $\dot{M}$, keeping the luminosity ratio of the BBB to the IR bump. Although this assumption is rather uncertain, it is worth noting that this component contributes not to band luminosity, but only to bolometric luminosity in the present study.

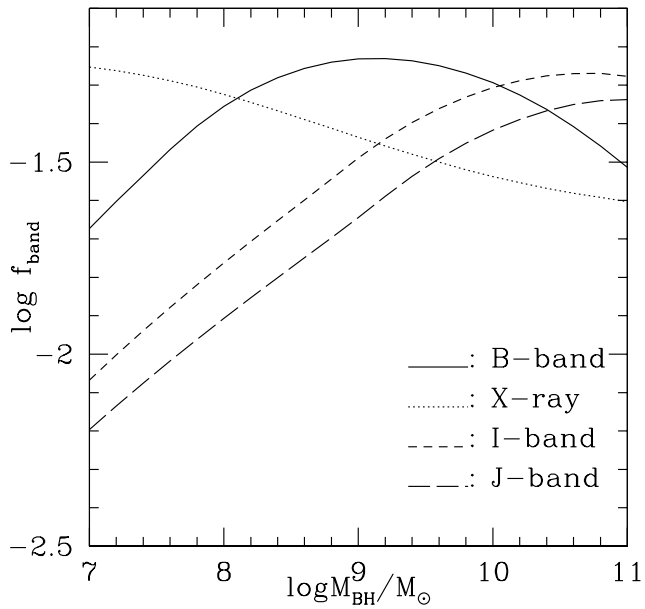

Fig. 2.. The fraction of the luminosity in each band among bolometric luminosity, $f_{\rm band}$, as a function of $M_{\rm BH}$ at $z = 3.0$ and $\dot{M} = 5.0 \times L_{\rm Edd}/c^2$. Line represent B-band(solid line), X-ray(dotted line), I-band(short dash line), and J-band(long dash line), respectively.

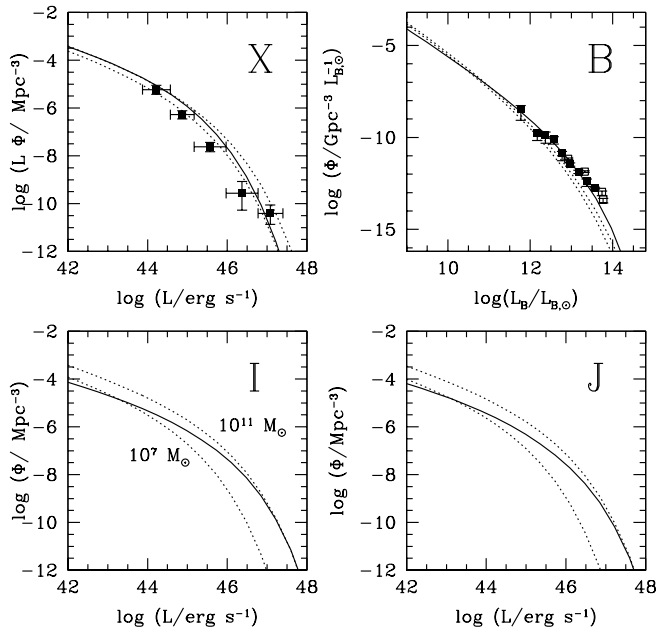

Fig. 3.. QSO Luminosity Functions calculated based on model A. Here, model parameters are $t_{\rm Q} = 4.0 \times 10^7$ yr, $\ell = 1$, and $C = 4.0 \times 10^8$. Note that $z = 3.5$ for X-ray *ROSAT* band, and otherwise $z = 3.0$. Top left; X-ray *ROSAT* band. The filled squares are data by Miyaji et al. (1998) for the redshifts of $2.3 < z < 4.6$. Top right; B-band. The filled squares are data by Pei (1995) for the redshifts of $2.5 < z < 3.5$. Bottom left; I-band. Bottom right; J-band. In each figure, dotted lines represent the case that QSOs have the same spectrum (and thus the same $f_{\rm band}$) as that for black hole mass of $M_{\rm BH} \simeq 10^7$ and $10^{11} M_\odot$ at $\dot{M} = 5.0 \times L_{\rm Edd}/c^2$ (see Figure 1), and the solid lines represent the case that each QSO has $M_{\rm BH}$-dependent spectrum.

3. QSO Luminosity Functions at $z \sim 3.0$

Once the spectra are given, we can calculate the fraction of the luminosity at a certain band among the bolometric one, $f_{\rm band} \equiv L_{\rm band}/L$. The previous models adopt the same spectral shape taken from the averaged observational one (e.g., Elvis et al. 1994) for wide ranges of $M_{\rm BH}$ and $\dot{M}$; that is, the value of $f_{\rm band}$ was kept constant. This treatment is, however, inappropriate, since QSO spectra should have some $M_{\rm BH}$ and $\dot{M}$ dependences as we saw in the previous subsection. In other words, $f_{\rm band}$ should change as a black hole grows and $\dot{M}$ decays with the time.

Figure 2. summarizes the resultant $f_{\rm band}$ in B-(4035 – 4765Å), I-(0.94 – 1.12 μm), J-bands(1.15 – 1.33 μm), and X-ray (0.5 – 2.0 keV, corresponding to the *ROSAT* energy band). This figure shows that in the I- and J-bands $f_{\rm band}$ decreases by one order of magnitude as $M_{\rm BH}$ decreases by four orders, whereas in the B-band and X-ray $f_{\rm band}$ varies less. This distinct behavior in the infrared bands compared with other bands arises from the fact that BBB spectral shape moves towards shorter wavelength with decreasing $M_{\rm BH}$ Accordingly, this produces interesting features in the shape of the LFs.

The theoretical QSO LFs can be calculated according to equation (9) for each waveband. As noted before, the parameters were determined such that the theoretical models should reproduce the observational, rest-waveband luminosity functions in B-band (Pei 1995) and in X-rays (Miyaji et al 1998). In the present study, we assume that the AGN obscuration play only a minor role in the high-z (> 1), high luminosity ($L_{\rm x} > 10^{44.5}$ erg s^{-1}) regimes for the following reasons. It is indeed true that there are several intrinsically obscured QSOs observed (obscured by some material, say, dusty tori and/or starburst regions surrounding the active nuclei). Brandt (1997) noted the existence of type 2 QSOs and Veilleux et al. (1999) pointed out that a part of ULIRG is the candidate for highly obscured QSOs. However, it is unlikely that they contribute significantly to the QSO LFs at the bright end, since Akiyama et al. (2000) reported that type 2 AGNs known to date are dominated by nearby low-luminous objects in 2 – 7 keV band (see their Fig.9). Further, they plot the redshift distributions of type 1/2 AGNs as functions of redshifts (see their Fig.10b). Then, they have calculated the expected redshift distribution of type 1 AGNs using the hard-band X-ray LFs of type 1 AGNs (Boyle et al.1998), finding that this expected distribution agrees with that of their samples of type 1 AGNs (obtained by ASCA Large Sky Survey) by the pos-

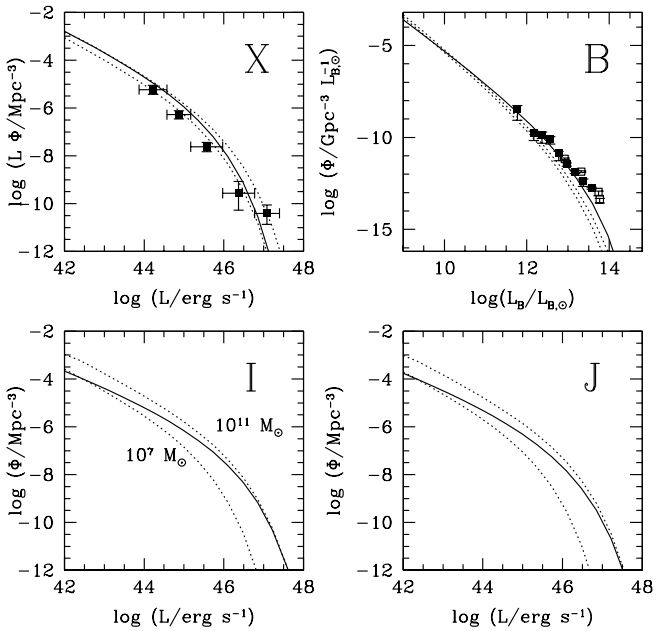

Fig. 4.. Same as figure 3. but for model B. Model parameters are $t_{\rm Q} = 3.5 \times 10^5$ yr, $\ell = 1$, and $\epsilon = 4.0 \times 10^{-4}$.

sibility of 64%. Next, they did the same but for type 2 AGNs assuming that the shape of LFs of type 2 AGNs is the same as that of type 1 AGNs. The expected number of the type 2 AGNs at $z > 0.4$ is about 10 among 30 identified AGNs in total, whereas there was no type 2 AGNs detection in their data at high redshift. That is, it is very unlikely that type 2 AGNs are distributed in the same way as that of type 1 AGNs; such a probability is only 5%. Certainly, there exists a deficiency of type 2 AGNs at $z > 0.4$, at least, in the high luminosity regimes. Still, we admit that the source number is insufficient to derive solid conclusion from their data. We should await further observational study to be conducted in near future.

In the present study, we thus consider only type 1 QSOs in the calculations of the QSO LFs to be compared with the observed QSO LFs. It is still possible that, depending on X-ray energy ranges, the fraction of type 2 AGNs may vary to some degree, giving rise to slightly different behavior in LFs at soft and hard X-ray bands. This issue will be discussed in a future paper.

The observed luminosity functions depend on the cosmological parameters (Hubble parameter, h, and the deceleration parameter, q_0), as well as the spectral index at the relevant bands (for K-correction). The dependence on h and q_0 is simple; $\Phi(L,z) \propto dV^{-1} d_L^{-2}$, $L \propto d_L^{-2}$ (here, dV is the comoving volume element, and d_L is the luminosity distance). As shown by Hartwik & Schade (1990), the dependence on α is comparatively large. Pei (1995) presents data only for $(h, q_0, \alpha) = (0.5, 0.5, 0.5)$ and $(h, q_0, \alpha) = (0.5, 0.1, 1.0)$. In our spectral model, α is nearly 1.0 in the B-band at redshift, $z \sim 3$. Thus, we modify Pei's data for $(h, q_0, \alpha) = (0.5, 0.1, 1.0)$ to satisfy ΛCDM. Since the observed optical and X-ray LFs are corrected with an assumed α of unity, which is equivalent to no K-collection, we calculate theoretical LFs at observer's frame. Once the parameters are determined by optical and X-ray LFs, then the luminosity function expected in the I- and J-band can be obtained.

Figure 3 and 4 represent the calculated luminosity functions for model A and model B, respectively. In all the panels of both figures, the dotted lines represent models assuming that all QSOs have the same spectrum as that with $M_{\rm BH}$ of 10^7 (lower line) or $10^{11} M_\odot$ (upper line) and $\dot{M}$ of $5.0 \times L_{\rm Edd}/c^2$, whereas the solid lines represent models that each QSO exhibits different spectra according to variations of black-hole mass.

As figures 3 and 4 show, the dotted lines nearly coincide with each other in X-ray and B-band, whereas they can be clearly separated in I- and J-band. In other words, LFs in X- and B-bands contain practically no information regarding black-hole mass, while LFs in NIR bands do. This can be explained in terms of the different behavior of $f_{\rm band}$ in those band, as are illustrated in figure 2. In the X- and B-band, $f_{\rm band}$ varies little (within a factor of $\sim$2), even if $M_{\rm BH}$ changes by four orders of magnitude, while in I- and J- bands $f_{\rm band}$ appreciably decreases (a factor of $\sim$ 10) as $M_{\rm BH}$ decrease. In the lower two panels of figures 3 and 4, especially, the solid line approaches the dotted line of $M_{\rm BH} = 10^{11} M_\odot$ on the higher luminosity side ($L_{\rm band} \gtrsim 10^{46}$ erg s^{-1}), whereas it approaches that of $M_{\rm BH} = 10^7 M_\odot$ on the lower luminosity side ($L_{\rm band} \lesssim 10^{44}$ erg s^{-1}). This clearly points that the more massive the black hole is, the brighter the QSO becomes at NIR bands (Figure 2).

The dotted lines in figures 3 and 4 are inconsistent with our model spectra, since those lines are plotted under the assumption that QSOs with different $M_{\rm BH}$ have the same spectral shape, while we expect $M_{\rm BH}$-dependence of the QSO spectrum as is demonstrated in figure 1. As mentioned before, the previous studies have used the one observational spectrum for all QSOs. In this sense, the dotted lines also represent the cases, in which the spectral shape is fixed as in the previous models (e.g. HL98, HNR98). The observational mean spectrum by Elvis et al (1994) is nearly equal to our spectrum model of $M_{\rm BH} \simeq 10^9 M_\odot$ and $\dot{M} = 5.0 \times L_{\rm Edd}/c^2$. The upper panels of figures 3 and 4 show that whichever model one may use, the previous model or our model, the luminosity functions hardly differ in B-band and X-ray. The lower panels, on the other hand, demonstrate that black-hole mass dependence of the QSO spectra manifests in the luminosity function in I- and J-band. Therefore, if QSO luminosity functions are observed at $z \sim 3$ in these wave bands in future, we can, in principle, constrain the $M_{\rm BH}$-

dependence of QSO spectrum, thus probing cosmological evolution of the black-hole mass in QSOs.

Despite the fact that QSO diminishing timescale is longer in model A ($t_{\rm Q} \sim 4.0 \times 10^7$ yr) than in model B (3.5×10^5 yr), these figures look very similar. This is because the mass fractions are different: $\epsilon = 4.0 \times 10^{-4}$ in model B, while in model A ϵ is not constant but around $\sim 10^{-5}$. Here, we note that if we use larger t_Q and smaller ϵ in model B, we cannot reproduce observed LFs. Since the inclination of LFs mainly depends on ϵ, theoretical LFs become more steeper with smaller ϵ.

Which value is more reasonable for ϵ? The ratio of the black-hole mass to the host halo mass (ϵ) is not directly observable, but MG98 suggest for the nearby galaxies and QSOs, the ratio of the central black-hole mass to the bulge mass is $M_{\rm BH}/M_{\rm bulge} \sim 0.006$. Then, the value of ϵ can be estimated through the baryon mass fraction in the total, $\Omega_{\rm b}/\Omega_0 \simeq 0.1$. If most of baryonic matter is contained in the bulge, we have $\epsilon \sim 10^{-3.0}$, more consistent with the Model B assumption. MG98 also support the linear $M_{\rm BH} - M_{\rm halo}$ relation, equation (4). On the other hand, Fukugita et al. (1998) noted that the bulge density is less than the baryon density by about one order of magnitude, $\Omega_{\rm bulge} = 0.1\Omega_{\rm b}$. If so, we have $\epsilon \sim 6 \times 10^{-5}$, in good agreement with the Model A assumption. More recently, Meritt & Ferrarese (2001) noticed the tight $M_{BH} - \sigma$ relation (with σ being halo velocity dispersion); $M_{\rm BH} \propto \sigma^{4.72}$, which is close to equation (3). They also show $M_{\rm BH}/M_{\rm bulge} \sim 0.0012$, which is by a factor of ~ 5 smaller than the value obtained by MG98 and could rule out model B. The similar conclusion was derived based on the mass estimate based on the reverbration mapping (Laor 1998).

Another parameter $t_{\rm Q}$ should also constrain models. By the usual picture of Eddington-limited accretion, black hole only grows as $M_{\rm BH} \propto \exp(t/t_{\rm Edd})$, where $t_{\rm Edd} \sim 3 \times 10^7$ yr is the *e-folding time*. As HNR98 mentioned, this supports Model A.

4. QSO Luminosity Functions at $z \sim 2$

Finally, we present the calculated LFs at intermediate redshifts. Here, we only display the cases with Model A, since Model B produces similar results except for the values of $t_{\rm Q}$ (see figures 3 and 4). Model parameters are $t_{\rm Q} = 4.0 \times 10^7$yr and $C = 4.0 \times 10^8$, which are the same as those in figure 3 ($z \sim 3.0$). Then, by setting ℓ to be a fitting parameter, we can well reproduce the observational QSO LF at $z = 2.0$ and $z = 1.3$, as are demonstrated in figure 5. Here, we let $\ell_{\rm x}$ and $\ell_{\rm B}$ be the initial Eddington ratios (ℓ) in X-ray and B-band, respectively. The best fit models give $(\ell_{\rm x}, \ell_{\rm B}) = (0.24, 0.66)$ at $z = 2.0$, and $(\ell_{\rm x}, \ell_{\rm B}) = (0.10, 0.25)$ at $z = 1.3$. Infrared LFs are calculated by using the same ℓ as those of B-bands and are displayed in figure 6.

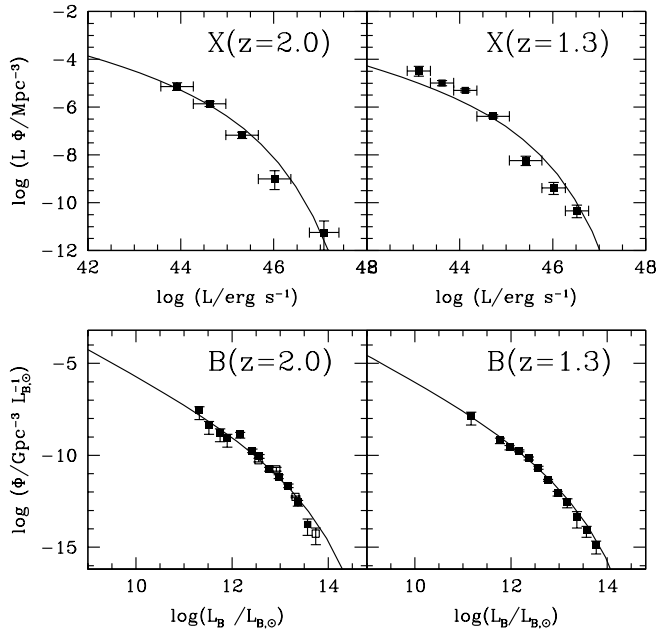

Fig. 5.. The same as figure 3 (model A) but at different redshifts: $z = 2.0$ (solid lines) and $z = 1.3$ (dashed lines), respectively. and in B-bands (top right). Model parameters are the same as those in figure 4 except for the initial Eddington ratios: $\ell_{\rm x} = 0.24$ ($z = 2.0$) and 0.10($z = 1.3$), and $\ell_{\rm B} = 0.66$ (left) and 0.25 (right). Also plotted are the observed LFs. The filled squares in the top left panel represent the observed LFs in X-ray *ROSAT* bands taken by Miyaji et al. (1998) at redshift of $1.6 < z < 2.3$ and at $0.8 < z < 1.6$, while the filled and open squares in the top right panel are data from Pei (1995) for the redshifts of $1.9 < z < 2.2$ and $1.2 < z < 1.4$.

Similar to figures 3 and 4, mass dependence of LFs at NIR bands is evident. The more luminous quasars are, the more massive become central black holes. As mentioned before, we have used the formation rate of dark halo by Kitayama & Suto (1996), instead the time derivatives of PS mass function. The distinction between the two is considerable in these redshifts: For example, in X-ray, PS mass function under-estimates the number densities of QSOs at $L_{\rm x} \leq 10^{44}$ergs^{-1} by a factor of 10 when we choose ℓ to fit LFs at higher $L_{\rm x}$ side. This is because on the lower $L_{\rm x}$ side, negative destruction rate domiates the time derivative of PS mass function.

Figure 7 plots the time evolution of the initial Eddington ratios. Our model requires $\ell_{\rm B}$ being about twice as much as $\ell_{\rm x}$ at both of $z = 2.0$ and $z = 1.3$, which contrasts the cases at $z \sim 3$, in which the same Eddington ratios, $\ell_{\rm B} = \ell_{\rm x} = 1$, can give reasonable fit to the observations. This implies that for lower mass-flow rates at relatively low redshifts X-ray radiation tends to be suppressed in the observations with respect to our modeled value for the same optical radiation. In other words, our model spectra may over-predict X-ray fluxes at $\ell \ll 1$, if the discrepancy in $\ell_{\rm B}$ and $\ell_{\rm x}$ is real. However, it is too

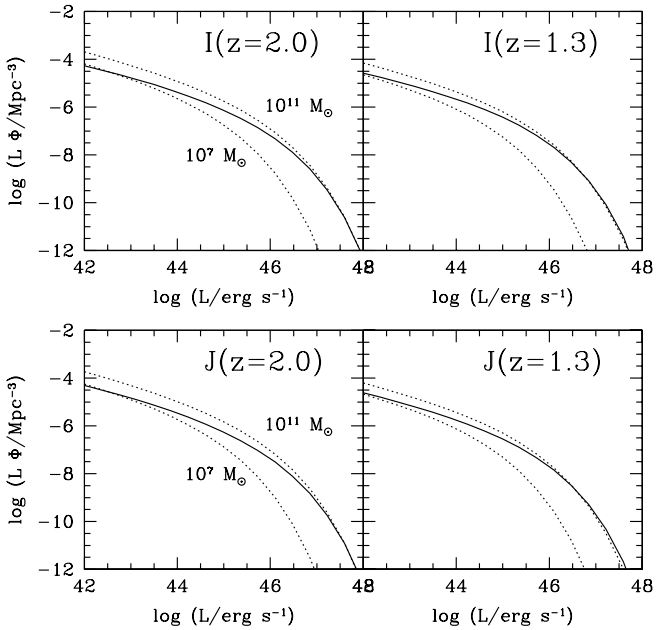

Fig. 6.. QSO LF at I- and J-band at intermediate redshift. Dotted lines represents the case that QSOs have the same spectrum as that for black hole mass of $M_{\rm BH} \simeq 10^7$and$10^{11}\,{\rm M}_\odot$ at $\dot{M} = 5.0 \times L_{\rm Edd}/c^2$. Here, we assume the initial Eddington ratio to be equal to that at B-band, $\ell = \ell_{\rm B}$.

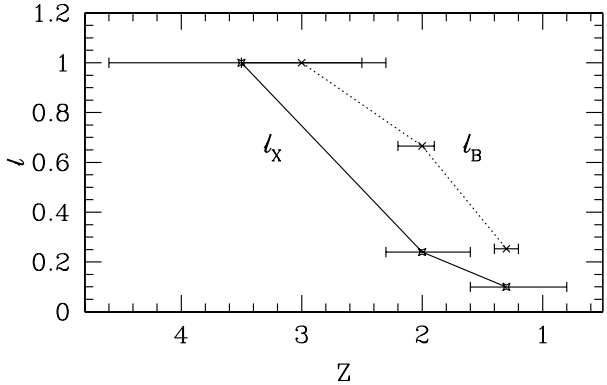

Fig. 7.. The time evolution of the best fitting initial Eddington ratios, $\ell_{\rm B}$(dotted line) and $\ell_{\rm x}$(solid line).

early to take this difference seriously, since the observational selection criteria of QSOs are somewhat different between X-ray and B-band LFs. Especially, error bars in X-ray are comparatively large, since smaller number of QSOs were used at X-ray LFs. We should await future intensive observations to be performed (see the next section for discussion).

Several issues still remain to be solved. First, the assumption of $\ell = 1.0$ at $z \sim 3.0$ may not be obvious. This is a naive expectation, and high redshift QSO survey may point that $\ell < 1.0$ even at $z \sim 3$. Next, we have not considered the time evolution of $t_{\rm Q}$ and ϵ. We also did not consider depletion of fuel mass (Kauffman, Haehnelt 2000; Cavaliere, Vittorini 2000). These evolution may explain decreasing LFs at $z \leq 2$ without the evolution of ℓ.

5. Discussion

We construct a simple model for LFs based on the previous models by HL98 and HNR98 but newly adopting the realistic disk spectra which have $M_{\rm BH}$ and $\dot{M}$ dependence. Our models for LFs can give reasonable fit to the observed LFs both in B-band and X-rays for redshift $z \sim 3$. We also show that these LFs are not sensitive to black-hole mass distribution in QSOs, but instead LFs at NIR, which will be available in the near future by IR QSO surveys, should contain information as to $M_{\rm BH}$.

Our model could also reproduce the shape of LFs at a variety of redshifts less than $z = 3.0$, however, we need to assume sub-Eddington initial luminosity of black holes at their formation epoch. This is consistent as the results obtained by Haiman & Menou (2000) who considered the B-band LFs only. From the semi-analytical approach for galaxy/QSO formation, Kauffmann & Haehnelt (2000) suggested that the sharp decline in QSO number densities from $z \sim 2$ to $z \sim 0$ results from a combination of three factors: (i) a decrease in the galaxy-galaxy merging rate, (ii) a consumption of gas due to star formation (corresponding to decreasing ℓ), and (iii) an adopted assumption of increasing accretion timescale (i.e., decreasing ℓ and increasing $t_{\rm Q}$).

Our model predicts $\ell_{\rm x} < \ell_{\rm B}$ by a factor of ~ 2.5. This may indicate that our model spectra overestimate X-ray flux at luminosity $L \ll L_{\rm Edd}$. In other words, we need to suppress X-ray flux compared with B-band one in the model spectra at low luminosities. This may require significant improvements of the model spectra adopted in the present study. Cosmological evolution of QSO spectrum requires further research. We also note that this may take part in the discrepancy of observed comoving density of QSOs at $z > 2.5$ between B-band and X-rays.

If QSO accretion-disks turn into the ADAF regime at low redshift due to low accretion rate (e.g., Yi 1996; Haiman & Menou 2000), optical radiation should be much suppressed compared with X-ray radiation; the broad-band spectrum of ADAF is generally harder than

the present disk-corona spectra, on the contrary to our results. Intrinsic dust extinction at (rest) optical/UV leads to the reduction in observed B-band luminosity, which again produces the opposite effect. Rather, our result may suggest a drastic shrinkage of the X-ray emitting region (probably accretion disk corona) at low luminosities. To probe this, we need more studies concerning the conditions creating and/or sustaining hot coronal flow above cool accretion disk.

In the present study, we calculated the formation rates of dark halos by the formalism based on PS mass function (PS halo), assuming each PS halo harbors only one black hole. Generally speaking, however, PS halos are not precisely equal to the galactic halos. For example, the mass scale of $M_{\rm halo} \sim 10^{14} M_\odot$ corresponds to a galaxy cluster and, hence, it is not correct to assume that such a huge PS halo contains only one black hole (this is known as the over-merging problem). Thus, we should be careful with the maximum halo mass $M_{\rm halo}$ used in the calculation of QSO LFs so as not to exceed a certain limit. At $z = 3.0$, the halos which mostly contribute to LFs at the bright end (for B-band, $L_{\rm B} \sim 10^{13.5} L_{\rm B,sun}$) have $M_{\rm halo} \sim 10^{13} M_\odot$, but at $z = 1.3$ the maximum halo mass attains $10^{14} M_\odot$. Therefore, our calculated LFs suffer over-merging problems only at higher luminosity side at lower redshift. But to evaluate ℓ, we can conclude that this effect is small.

Throughout the present study, we assume that each dark halo contains only one massive black hole whose mass is scaled with the host dark-halo mass. It is interesting to note recent discovery of multiple, intermediate-mass black holes being created in post-starburst regions in M82 (Matsumoto & Tsuru 1999; Matsushita et al. 2000). This is not consistent with our assumption, but it may be that such intermediate-mass black holes will eventually merge into one big hole within timescales much shorter than the Hubble time.

The authors would like to express their thanks to Dr T. Miyaji for providing the electric data of the ROSAT Luminosity Functions.

This work was supported in part by Research Fellowships of the Japan Society for the Promotion of Science for Young Scientists (4616, TK).

References

Akiyama et al. 2000, ApJ 532, 700A
Abramowicz M., Chen X., Kato S., Lasota J.-P., Regev O. 1995, ApJ 438, L37
Bertschinger E. 1985, ApJS 58, 39
Boller Th., Brandt W.N., Fink H.H. 1996, A&A 305, 53
Boyle B.J., Shanks T., Peterson B.A. 1988, MNRAS 235, 935
Boyle B.J., Georgantopoulos,I., Blair,A.J., Stewart,G.C., Griffiths,R.E., Shanks,T., Gunn,K.F., & Almaini,O. 1998, MNRAS 296, 1
Brandt W.N., Mathur S., Elvis M. 1997, MNRAS 285, L25
Brandt, W. N., et al. 1997, MNRAS 290, 617
Cavaliere A., Szalay A.S. 1986, ApJ 311, 589
Cavaliere A., Vittorini V. 1998, in ASP Conf. Ser. 146, The Young Universe: Galaxy Formation and Evolution at Intermediate and High Redshift, ed. S. D'Odorico, A. Fontana, & E. Giallongo (ASP: San Francisco), p26
Cavaliere A., Vittorini V. 2000, ApJ 543, 599
Connolly A. Szalay A.S., Dickinson M., Subbarao M.U., Brunner R.J. 1997, ApJ 486, L11
de Bernardis P. et al. 2000, Nature 404, 955
Efstathiou G., Rees M.J. 1988, MNRAS 230, 5p
Ferrarese L., Merritt D. 2000, ApJ 539, L9
Elvis M. et al. 1994, ApJS 95, 1
Fontana A. et al. 1998, AJ 115, 1225
Franceschini A., Hasinger G., Miyaji T., Malquoli D. 1999 MNRAS 310, L5
Fukugita et al. 1998, ApJ 503, 518
Gebhardt et al. 2000, ApJ 539, L13
Grazebrook K. et al. 1999, MNRAS 306, 843
Haardt F., Maraschi L. 1991, ApJ 380, L51
Haehnelt M.G., Natarajan P., Rees M.J. 1998, MNRAS 300, 817 (HNR98)
Haehnelt M.G., Rees M.J. 1993, MNRAS 263, 168
Haiman Z., Loeb A. 1998, ApJ 503, 505 (HL98)
Haiman Z., Loeb A. 1999, ApJ 521, L9 (HL99)
Haiman Z., Menou K. 2000, ApJ 531, 42
Ichimaru S., 1977, ApJ 214, 840
Kauffman G., Haehnelt M.G. 2000, MNRAS 311, 576
Kawaguchi T., Shimura T., Mineshige S. 2001, ApJ 546, 966
Kitayama T., Suto Y. 1996, MNRAS 280, 638
Kobayashi Y., Sato S., Yamashita T., Shiba H. & Takami H. 1993, ApJ 404, 94
Kormendy J., Richstone D. 1995, ARA&A 33, 581
Lacey C.G., Cole S. 1993, MNRAS 262, 627
Laor A. 1998, ApJ 505, L83
Laor A., Fiore F., Elvis M., Wikes B. J., McDowell J. C. 1997, ApJ 477, 93
Macleod et al. 1999, ApJ 511, L67
Madau P. et al. 1996, MNRAS 283, 1388
Magorrian J. et al. 1998, AJ 115, 2285 (MG98)
Manmoto T., Kusunose M., Mineshige S. 1997, ApJ 489, 791
Matsumoto H., Tsuru T. G. 1999, PASJ 51, 321
Matsushita S. et al. 2000, ApJ 545, L107
Mcleod et al. 1999, ApJ 511, L67
Mineshige S., Kawaguchi T., Takeuchi M., Hayashida K. 2000, PASJ 52, 499
Miyaji T., Hasinger G., Schmidt M. 1998, in Proc. Highlights in X-Ray Astronomy (astro-ph/9809398)
Miyaji T., Hasinger G., Schmidt M. 2000, A&A 353, 25
Narayan R., Yi I. 1994, ApJ 482, L13
Neugebauer G. et al. 1987, ApJS, 63, 615
Nulson P.F.J., Fabian A.C 2000, MNRAS 311, 346
Osmer P.S. 1982, ApJ 253, 28
Otani C., Kii T., Miya K. 1996 in Röntgenstrahlung from the Universe (MPE Report 263), ed H.U. Zimmermann, J.E. Trümper, H. Yorke (MPE Press, Garching) p491
Pei Y.C. 1995, ApJ 438, 623
Polletta, M. & Courvoisier, T.J.-L. 1999, A&A, 350. 765

Pounds K.A., Done C., Osborne J. 1996, MNRAS 277, L5
Press W.H., Schechter P.L. 1974, ApJ 181, 425
Radovich M., Klaas U., Acosta-Pulido J. & Lemke D. 1999, AA, 348, 705
Rees M.J. 1984 ARA&A 22, 471
Rees M.J., Blandford R.D., Begelman M.C., Phinney S. 1982, Nature 295, 17
Sasaki S. 1994, PASJ 46, 427
Schmidt M., Green R.F. 1983, ApJ 269, 352
Shakura N.I., Sunyaev R.A. 1973, A&A 24, 337
Shaver P.A. et al. 1996, Nature, 384, 439
Shaver P.A., Hook I.M., Jackson C.A., Wall J.V., Kellermann K.I. 1999 in Highly Redshifted Radio Lines, eds. C. Carilli et all. (PASP: San Francisco), p163
Steidel et al. 1999, ApJ 519, 1
Stengler-Larrea, E. A. et al. 1995, ApJ 444, 64
Telesco C.M., Becklin E.E., Wynn-Williams C.G. & Harper D.A. 1984 ApJ 282, 427
Veilleux, S., Sanders, D. B., & Kim, D.-C. 1999, ApJ 522, 139
Yi I. 1996, ApJ 473, 645
Zheng W., Kriss G.A., Telfer R.C., Grimes J.P., Davidsen A.F. 1997, ApJ 475, 469